Diffusion-controlled reactions with a binding site hidden in a channel

Leonardo Dagdug and Alexander Berezhkovskii[a)]
Mathematical and Statistical Computing Laboratory, Center for Information Technology, Bethesda, Maryland 20892

Sergey M. Bezrukov
Laboratory of Physical and Structural Biology National Institute of Child Health and Human Development National Institutes of Health, Bethesda, Maryland 20892 and St. Petersburg Nuclear Physics Institute, Gatchina 188350, Russia

George H. Weiss
Mathematical and Statistical Computing Laboratory, Center for Information Technology, Bethesda, Maryland 20822

(Received 8 July 2002; accepted 4 November 2002)

The rate of a diffusion-controlled reaction with a buried binding site is smaller than the rate for the same site on the surface. We study the slowdown of the reaction rate when the site is hidden in a pore that connects two bulk media. On the assumption that the pore is cylindrical we derive an expression for the Laplace transform of the rate coefficient from which we infer the long-time limit of the reaction rate. This provides information on how the reaction rate depends on the channel radius, the location of the site, and the diffusion constant in the pore, which is allowed to differ from that in the bulk. The validity of approximations was checked by simulations that indicated excellent agreement between the analytical and and numerical results. © *2003 American Institute of Physics.* [DOI: 10.1063/1.1533061]

I. INTRODUCTION

Diffusion-controlled reactions of solutes with a reaction site hidden in a protein membrane channel or protein cavity underlie many basic biological processes. A set of well-studied examples is provided by ligand activation of water soluble and integral membrane proteins in intra- and extracell signal transduction, where structural studies often reveal clefts or pockets for ligand-binding sites.[1–3] Noncompetitive inhibition of ion channels in synaptic transmission is another example in which entrance into the pore and diffusion in the pore are essential steps of the inhibition reaction.[4] Importantly, noncompetitive inhibitors that block open ion channeels are considered to be promising neuroprotective agents against glutamate excitoxicity in a number of neurodegenerative disorders.[5–7]

Diffusion to a hidden reaction site is able to slow down the binding reaction by many orders of magnitude. This is one of the conclusions of a recent single-molecule study of the translocation of antibiotics through a bacterial porin, OmpF.[8] Experimental results indicate that the on-rate of ampicillin binding to a constellation of charges in the constriction zone of the OmpF pore is about 1.3×10^4 $(\mathrm{M}\cdot\mathrm{s})^{-1}$. This represents a reduction of several orders of magnitude in the on-rate as compared to the rate expected for a binding site exposed on the surface. Though many factors may be responsible for this dramatic reduction, the diffusion step to the reaction site hidden in the center of the channel is a likely candidate.

In this paper we develop a theory of diffusion-controlled reactions when a reaction site is hidden in a membrane channel. A simple model of such a reaction is one in which it is assumed that the reaction site is located in a cylindrical channel of radius a, in the geometry shown in Fig. 1. The reaction will be said to occur when the first particle reaches the reactive site. Particles diffuse in the bulk and within the channel with the diffusion constants D_b and D_{ch}, respectively. Initially the concentration of particles in the bulk is constant and equal to c, and there are no particles in the channel. To initiate the reaction process the two openings of the channel are opened at $t=0$, permitting the particles to move into the cylinder.

It has been shown that, to a good approximation, diffusion in the channel can be described as being one-dimensional.[9–11] It will be assumed, in the framework of this one-dimensional description, that the reaction site can be modelled as a perfectly absorbing point. The survival probability of the site is the probability that the site has not been reached by particles entering the channel either from the left or right (Fig. 1). Since diffusing particles cannot cross the site, the survival probability is a product of two survival probabilities, found by solving an auxiliary problem. In this problem a perfectly absorbing site is located at the bottom of a cylinder of radius a and of length L. The study of this problem is the main focus of the present paper. We derive an analytical expression for the reaction rate as a function of L and a as well as diffusion constants in the bulk and inside the cylinder. When $L=0$ the problem reduces to a well-known one in which an absorbing disk is placed on a reflecting wall. This problem has been analyzed by a number of investigators.[12–16]

[a)]Permanent address: Karpov Institute of Physical Chemistry, 10 Vorontsovo Pole Street, 103064, Moscow K-64, Russia.

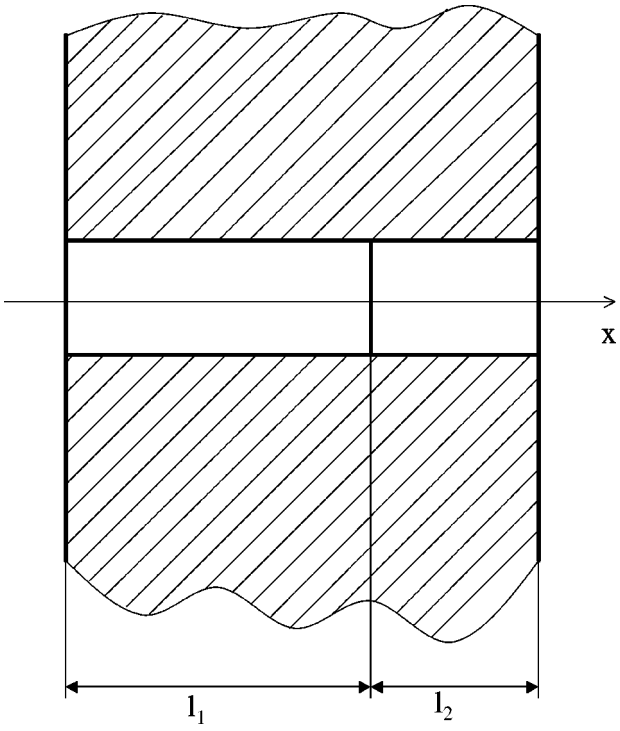

FIG. 1. Schematic diagram of the channel with a binding site. The site is located at distances l_1 and l_2 from the channel entrances, as shown.

The rate constant for a buried reaction site was first considered by Samson and Deutch who studied ligand binding to a reaction site buried inside an enzyme or protein.[17] Using a sophisticated but approximate analysis they derived an analytical expression for the rate constant in a spherical geometry in which a binding site is located at a specified depth in an otherwise reflecting sphere. In this paper we consider a simpler geometry allowing us to solve the problem by elementary means. These enable us to find not only the steady-state rate constant but also the time-dependent rate coefficient. The relation between the Samson–Deutch model and the present one is discussed in Sec. IV after we develop a theory for our model in the following section and compare our theoretical predictions with simulation results in Sec. III.

II. THEORY

The survival probability, $S_L(t)$, i.e., the probability that no particle has reached the reactive site at the bottom of the cylinder by time t, is given by

$$S_L(t)=\exp\left[-c\int_0^t k_L(\xi)d\xi\right], \tag{2.1}$$

where $ck_L(t)$ is a time-dependent flux of particles through the reactive site at time t. The object of our analysis is to determine $k_L(t)$ as a function of the parameters a and L as well as the two diffusion constants D_b and D_{ch}. In the final section we use Eq. (2.1) to express the survival probability of the binding site in the channel where the site can be reached by diffusing particles that enter the channel through either of the two ends.

To find $k_L(t)$ one has to solve the problem in three dimensions in the cylinder and in the bulk and match the two solutions at the entrance to the cylindrical pore. This program cannot be carried out due to its mathematical complexity. However, an approximate, but quite accurate, technique has recently been found to handle such problems.[9] The results of that reference show that the three-dimensional motion inside a cylinder in contact with a bulk can be treated as being one-dimensional diffusion, provided that the proper radiation boundary condition is imposed at the entrance to the cylinder. Results of extensive simulations using the accurate geometry, i.e., with a three-dimensional cylindrical channel in contact with the bulk were compared to those derived on the basis of the one-dimensional approximation in Refs. 9 and 11. Excellent agreement was found between the theoretically predicted results and those found in simulation for all values of the ratio L/a that determine the channel geometry.

Since diffusion in the channel can be described as one dimensional, the particle density at time t, $p(x,t)$, satisfies

$$\frac{\partial p}{\partial t}=D_{\mathrm{ch}}\frac{\partial^2 p}{\partial x^2},\quad 0<x<L \tag{2.2}$$

subject to the initial condition $p(x,0)=0$. The existence of a binding site at $x=L$ is translated into the absorbing boundary condition $p(L,0)=0$. It has been shown in Ref. 9 that the point $x=0$, as viewed from the cylinder, can be regarded as a partially absorbing boundary. To write the boundary condition at $x=0$ we introduce the flux of particles that enter the cylinder from the bulk at time t, $J_b(t)$. The boundary condition can then be expressed as

$$D_{\mathrm{ch}}\left.\frac{\partial p(x,t)}{\partial x}\right|_{x=0}=\kappa p(0,t)+J_b(t), \tag{2.3}$$

where the rate constant κ characterizes the efficiency of escape from the cylinder of a particle that approaches the boundary, and has been shown to be[9]

$$\kappa=\frac{4D_b}{\pi a}. \tag{2.4}$$

The function $J_b(t)$ in Eq. (2.3) is the flux of particles impinging on a disk of radius a on an otherwise planar reflecting wall. A boundary condition more accurate than Eq. (2.3) can be shown to be non-Markovian,[9] but reduces to Eq. (2.3) on time scales larger than a^2/D_b. At such times, $J_b(t)$ can be set equal to its stationary value, $4D_bac$. In our later analysis we will neglect details of the kinetics occuring on times of the order of a^2/D_b.

The rate coefficient is expressed in terms of $p(x,t)$ by

$$k_L(t)=-\frac{D_{\mathrm{ch}}}{c}\left.\frac{\partial p(x,t)}{\partial x}\right|_{x=L}. \tag{2.5}$$

To calculate $k_L(t)$ we consider the behavior of a particle that enters the cylinder at $t=0$ and calculate the flux that escapes through the reactive site at $x=L$ due to this particle. The motion inside the cylinder is described by a propagator $G(x,t|0)$ which satisfies the diffusion equation in Eq. (2.2) together with the boundary condition $G(L,t|0)=0$. How-

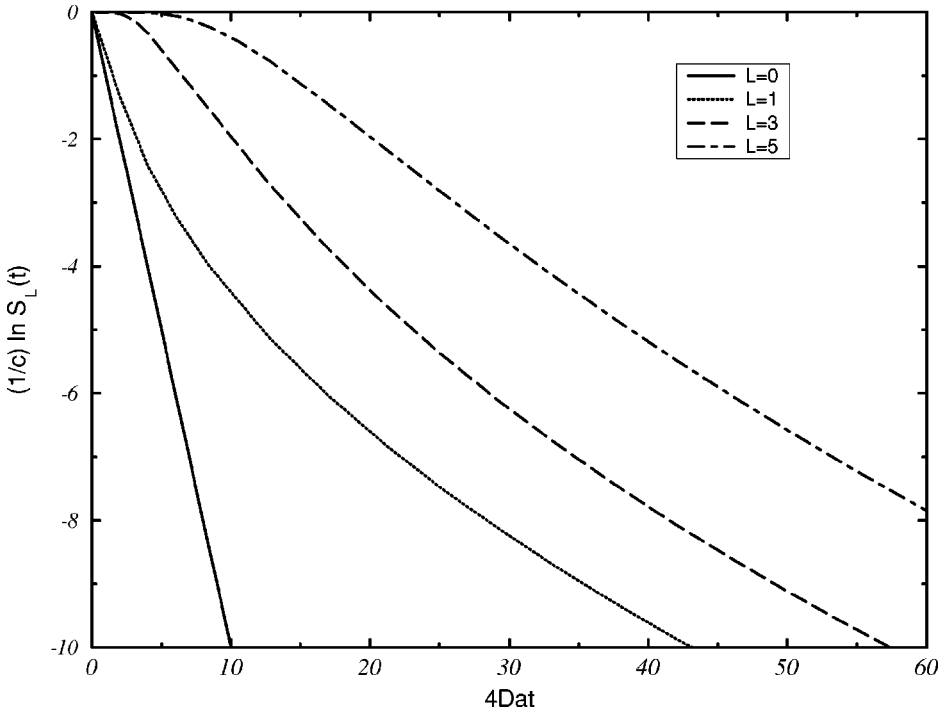

FIG. 2. Curves illustrating slowdown of the reaction rate due to hiding of the binding site in the cylinder. The solid line is the logarithm of the survival probability for a site exposed on the reflecting surface. The remaining lines give similar dependences for the reaction site hidden at the bottom of cylinders with different lengths L. The curves were obtained by numerical inversion of the Laplace transform $\hat{k}_L(s)/s$ using the expression for $\hat{k}_L(s)$ in Eq. (2.11).

ever the initial condition is now changed to $G(x,0|0)=\delta(x)$ and the boundary condition in Eq. (2.3) is also changed to

$$D_{\rm ch}\left.\frac{\partial G(x,t|0)}{\partial x}\right|_{x=0}=\kappa G(0,t|0). \tag{2.6}$$

The flux escaping through the reactive site, denoted by $f(t)$, is given by

$$f(t)=-D_{\rm ch}\left.\frac{\partial G(x,t|0)}{\partial x}\right|_{x=L}. \tag{2.7}$$

Then the rate coefficient can be expressed as

$$k_L(t)=4D_b a\int_0^t f(\xi)d\xi. \tag{2.8}$$

The analysis is best presented in terms of Laplace transforms. The Laplace transform of $k_L(t)$ is

$$\hat{k}_L(s)=\int_0^\infty e^{-st}k_L(t)dt$$

$$=4D_b a\frac{\hat{f}(s)}{s}=\frac{-4D_b D_{\rm ch}a}{s}\left.\frac{\partial\hat{G}(x,s|0)}{\partial x}\right|_{x=L}. \tag{2.9}$$

The equation satisfied by $G(x,t|0)$ can be solved by means of Laplace transforms. It is convenient to introduce a dimensionless combination, $\sigma=L^2s/D_{\rm ch}$. The Laplace transform of $G(x,t|0)$ is found to be

$$\hat{G}(x,s|0)=\frac{\sinh\left[\left(1-\frac{x}{L}\right)\sqrt{\sigma}\right]}{(D_{\rm ch}/L)[\sqrt{\sigma}\cosh(\sqrt{\sigma})+\kappa\sinh(\sqrt{\sigma})]}. \tag{2.10}$$

This leads to the following representation of $\hat{k}_L(s)$:

$$\hat{k}_L(s)=\frac{4D_b a}{(L^2/D_{\rm ch})\sqrt{\sigma}\left[\sqrt{\sigma}\cosh(\sqrt{\sigma})+\frac{\kappa L}{D_{\rm ch}}\sinh(\sqrt{\sigma})\right]}. \tag{2.11}$$

It follows from this that when $L=0$ the rate coefficient is $4D_b a$ as in Refs. 12–14. The slow down of the reaction rate due to the fact that $L\neq 0$ is illustrated in Fig. 2 for $D_b=D_{\rm ch}=D$. The curves were obtained by numerically inverting $\hat{k}_L(s)/s$ using the expression for $\hat{k}_L(s)$ given in Eq. (2.11). The numerical inversion was performed by the program Scientist (MicroMath Scientific Software, 1995) which uses two different methods to perform the inversion. Both of these produced the same results.

The long-time limit, $k_L(\infty)$, is found by passing to the limit $\sigma\to 0$ in Eq. (2.11). This yields the expression

$$k_L(\infty)=\frac{4D_b a}{1+\frac{\kappa L}{D_{\rm ch}}}=\frac{4D_b a}{1+\frac{4D_b L}{\pi D_{\rm ch}a}} \tag{2.12}$$

which obviously depends both on D_b and $D_{\rm ch}$. Initially, the rate coefficient is equal to zero since no particle is found in the cylinder. The short-time behavior can be determined by passing to the limit $\sigma\to\infty$ in Eq. (2.11). This leads to the approximation

$$k_L(t)\approx 16D_b a\sqrt{\frac{D_{\rm ch}t}{\pi L^2}}\exp\left(-\frac{L^2}{4D_{\rm ch}t}\right). \tag{2.13}$$

A solution for $k_L(t)$ for all values of t and for arbitrary values of the parameters can be found by numerically inverting $\hat{k}_L(s)$.

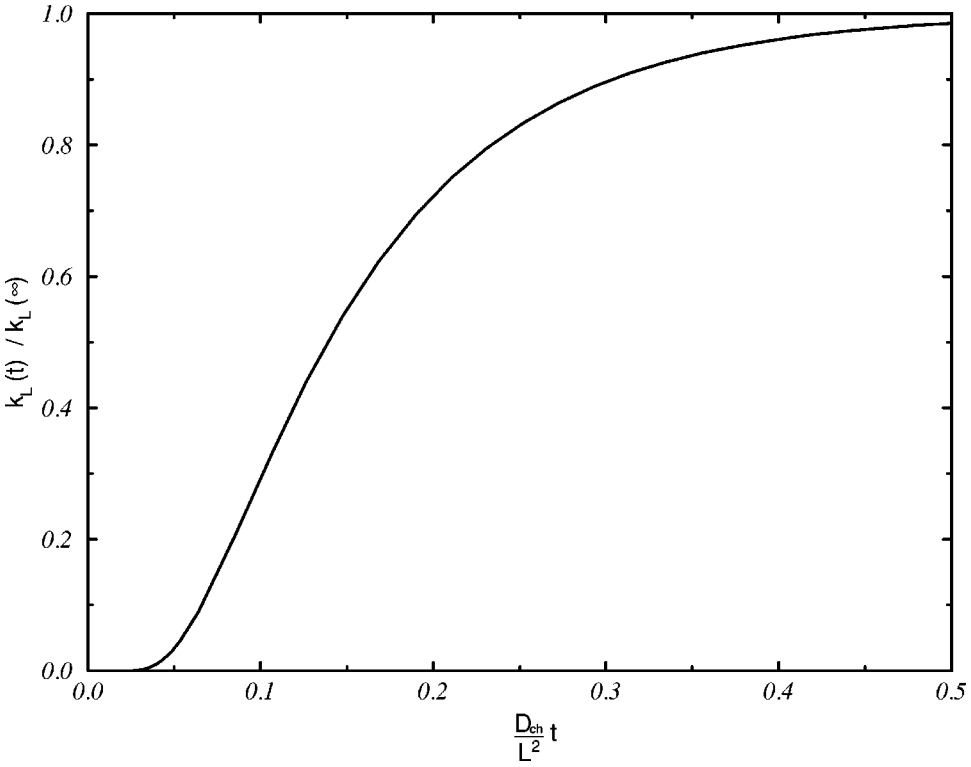

FIG. 3. Relaxation of the rate constant $k_L(t)$ to its plateau value $k_L(\infty)$ when the binding site is hidden in a long and narrow cylinder of length L. The dependence is calculated from Eq. (2.16) with $\tau = D_{\rm ch}\, t/L^2$.

When the cylinder is long and narrow, in the sense that $L \gg aD_{\rm ch}/D_b$, an approximate solution for $k_L(t)$, valid for all times, can be found. This solution is

$$k_L(t) \approx a^2 \sqrt{\frac{4\pi D_{\rm ch}}{t}} \sum_{n=0}^{\infty} \exp\left[-\frac{(n+1/2)^2 L^2}{D_{\rm ch}\, t} \right]. \qquad (2.14)$$

As might be anticipated this $k_L(t)$ depends only on properties of the cylinder and there is no effect of diffusion in the bulk on it. In the long-time limit, $k_L(t)$ takes the form

$$k_L(\infty) \approx \pi D_{\rm ch}\, a^2/L \qquad (2.15)$$

which is proportional to a^2 and not to a as is the case when $L=0$. Using the dimensionless time $\tau = D_{\rm ch}\, t/L^2$ we can write

$$\frac{k_L(t)}{k_L(\infty)} = \frac{2}{\sqrt{\pi \tau}} \sum_{n=0}^{\infty} \exp\left[-\frac{(n+1/2)^2}{\tau} \right]. \qquad (2.16)$$

A plot of this ratio is shown in Fig. 3.

III. SIMULATION RESULTS

Brownian dynamics simulations were run in a real three-dimensional geometry to check the accuracy of the theory outlined in the last section. The diffusion constants in the cylinder and in the bulk were set equal in our simulations, $D_b = D_{\rm ch} = D$. A further discussion of the simulations is to be found in the Appendix. We found very good agreement between the theoretically predicted values of $k_L(\infty)$ and that obtained by simulation. The relative discrepancy between the theory and simulations was less than 3 percent for all values of a and L used for simulations. A more detailed set of results are shown in the graphs in Figs. 4 and 5.

Figure 4 is a plot of the ratio $k_L(\infty)/4D_b a$ as a function of L/a, which is compared to the theoretical dependence given in Eq. (2.12). This dependence is indicated in Fig. 4 by the solid line, while the crosses correspond to the simulation results. There is close agreement between the two.

For the dependence of $k_L(\infty)$ on the radius of the cylinder, the theory predicts [cf. Eq. (2.12)] a transition from the linear behavior $k_L(\infty) = 4D_b a$ when $L \ll a$ to quadratic behavior given in Eq. (2.15) for long cylinders, $a \ll L$. This transition is illustrated by the curves shown in the inset in Fig. 5 for cylinders with $L = 0, 0.1$, and 1. A comparison of the theoretical prediction and numerical results is also shown in Fig. 5 for the cylinder with $L=1$ and $a = 0.02$, 0.03, 0.04, and 0.05. Again, there is excellent agreement between theory and the results of simulation.

IV. DISCUSSION

It is interesting to compare our result for the plateau value of the rate constant, $k_L(\infty)$, in Eq. (2.12) with the rate constant derived by Samson and Deutch,[17] for their model of diffusion-limited ligand binding to a reaction site buried inside of an enzyme or protein as shown in Fig. 6. This model reduces to ours with $D_{\rm ch} = D_b = D$ in the limit $R \to \infty$ at fixed values of the parameters a and L (Fig. 6). It is convenient to consider $1/k_L(\infty)$ which can be written as

$$\frac{1}{k_L(\infty)} = \frac{1}{k_{\rm disk}} + \frac{L}{\pi a^2 D} = \frac{1}{4aD} + \frac{L}{\pi a^2 D}, \qquad (4.1)$$

where $k_{\rm disk} = 4aD$ is the rate constant for a perfectly absorbing disk on an infinite reflecting plane, derived by Hill,[12] and Berg and Purcell.[13]

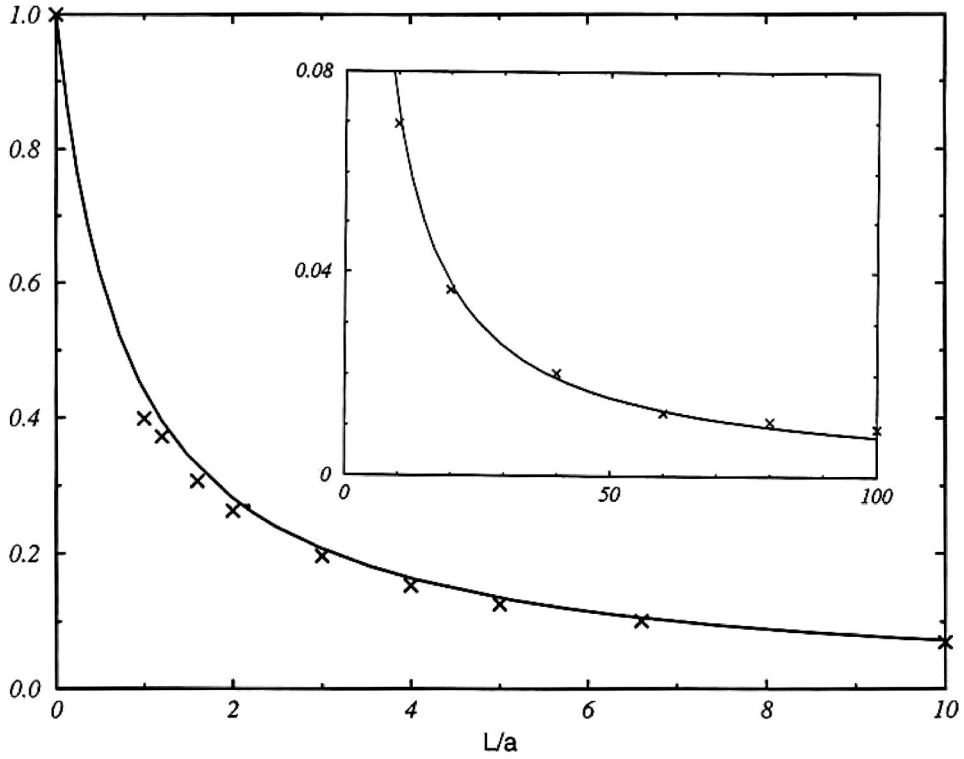

FIG. 4. The ratio of the plateau value of the rate coefficient for the binding site hidden in the cylinder of length L, $k_L(\infty)$, to the rate constant for the same site exposed on the reflecting surface, $4Da$. The plots are shown as a function of L/a. The solid curve is calculated from Eq. (2.12) with $D_b = D_{\mathrm{ch}} = D$. The crosses represent simulated data.

The inverse of the rate constant derived by Samson and Deutch (SD) in Ref. 17 can be written

$$\frac{1}{k_{\mathrm{SD}}(\theta_0, L|R)} = \frac{1}{k_{\mathrm{SD}}(\theta_0, 0|R)} + \frac{L}{2\pi R(R-L)(1-\cos\theta_0)} \tag{4.2}$$

in the notation used in Fig. 6. Here, $k_{\mathrm{SD}}(\theta_0, 0|R)$ is the SD expression for the rate constant for a circular absorbing spot on the surface of an otherwise reflecting sphere of radius R. It is

$$k_{\mathrm{SD}}(\theta_0, 0|R) = \frac{2\pi DR(1-\cos\theta_0)}{\eta(\cos\theta_0)} \tag{4.3}$$

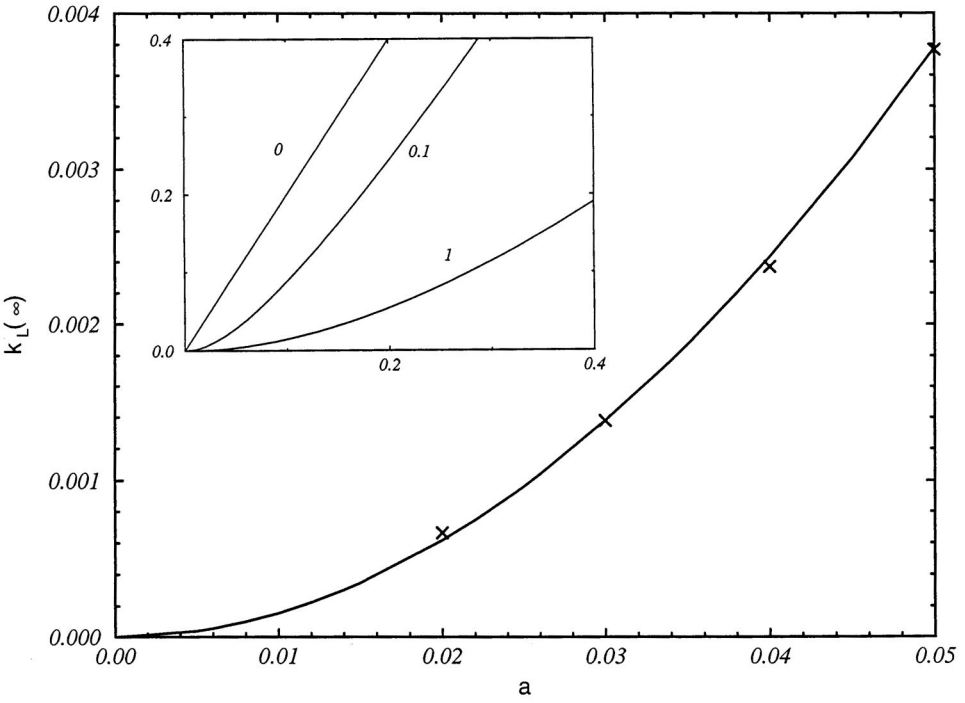

FIG. 5. Behavior of the plateau value of the rate coefficient, $k_L(\infty)$, as a function of the cylinder radius a for different values of L. The dependence is linear when the binding site is exposed on the reflecting surface. When the site is hidden in the cylinder the dependence is initially quadratic, becoming linear when the radius of the cylinder is larger than the cylinder length, as shown in the inset. The numbers near the curves indicate the cylinder length. Both the rate constant and the cylinder length and radius are expressed in dimensionless units. The curves are calculated from Eq. (2.12) with $D_b = D_{\mathrm{ch}} = 1/2$ in dimensionless units. The crosses in the main part of the figure were obtained from simulated data for a cylinder with $L = 1$ and the corresponding theoretical curve is drawn as a solid line.

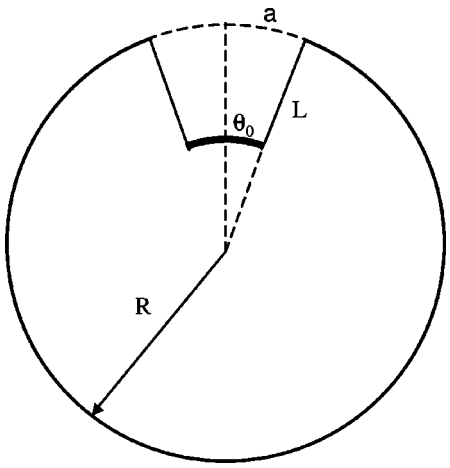

FIG. 6. A sketch of the model analyzed by Samson and Deutch, consisting of a reflecting sphere of radius R with a conical channel of length L that leads to the binding site indicated by the thick line. The channel opening is defined by the angle θ_0 and the arc length is equal to a.

in which $\eta(\cos\theta_0)$ is defined by

$$\eta(\cos\theta_0)=\frac{1}{2}\Bigg[1-\cos\theta_0+\sum_{l=1}^{\infty}\frac{P_{l-1}(\cos\theta_0)-P_{l+1}(\cos\theta_0)}{l+1}\Bigg], \quad (4.4)$$

where $P_l(\cos\theta_0)$ is the lth order Legendre polynomial.

When R is large and a is fixed so that $\theta_0=a/R$ the rate constant in Eq. (4.3) can be approximated by the rate constant for an absorbing disk on an infinite reflecting plane derived by Shoup, Lipari, and Szabo.[18] They applied the SD approach to this problem and found

$$k_{\mathrm{disk,SD}}=\pi aD. \quad (4.5)$$

One can find this result from Eqs. (4.3) and (4.4) by making use of the sum

$$\sum_{l=1}^{\infty}\frac{P_{l-1}(\cos\theta_0)-P_{l+1}(\cos\theta_0)}{l+1}=2\Bigg\{\sin\left(\frac{\theta}{2}\right)+\cos^2\left(\frac{\theta}{2}\right)\ln\left[1+\sin\left(\frac{\theta}{2}\right)\right]-\sin^2\left(\frac{\theta}{2}\right)\left[1-\ln\left[\sin\left(\frac{\theta}{2}\right)\right]\right]\Bigg\} \quad (4.6)$$

that can be derived using some relations from Ref. 19. The rate constant in Eq. (4.5) is smaller than the exact $k_{\mathrm{disk}}=4aD$ as must be the case because $k_{\mathrm{disk,SD}}$ is derived using an absorbing boundary condition (i.e., requiring the ligand concentration to vanish) only at one point at the center of the disk. The exact k_{disk}, on the other hand, is derived with an absorbing boundary condition on the entire disk surface.

The second term on the right-hand side of Eq. (4.2) takes the form $L/(\pi a^2D)$ in the large-R limit and with $\theta_0=a/R$. This coincides with the second term in Eq. (4.1). In the limits just mentioned we have

$$\frac{1}{k_{\mathrm{SD}}(\theta_0=a/R,L|R)}=\frac{1}{k_{\mathrm{disk,SD}}}+\frac{L}{\pi a^2D}=\frac{1}{\pi aD}+\frac{L}{\pi a^2D}. \quad (4.7)$$

A comparison of this formula and Eq. (4.1) indicates that the difference between the two rate constants is due to the difference between $k_{\mathrm{disk,SD}}$ and the exact value of k_{disk} as derived by Hill,[12] and Berg and Purcell.[13] This difference manifests itself only for very short cylinders, i.e., $L<a$. In the interesting case of the long cylinder, $L\gg a$, both approaches lead to the steady-state rate constant $\pi a^2D/L$.

Our analysis has the advantage of leading not only to the long-time plateau value of the rate coefficient, but also to the Laplace transform of the time-dependent rate coefficient. We were able to invert this transform in the most interesting case of a long, narrow cylinder, allowing us to give the explicit formula for $k_{\mathrm{L}}(t)$ in Eq. (2.14). This is possible because we have analyzed a simpler geometry than in the SD model.

V. A CONCLUDING REMARK

Two main results of the present paper are the expressions for the Laplace transform of the rate coefficient given in Eq. (2.11) and for the plateau value $k_L(\infty)$ given in Eq. (2.12). It allows one to analyze the dependence of the rate constant and the associated survival probability on the parameters a and L of the cylinder, and the diffusion constants D_{ch} and D_b. When the form of $S_L(t)$ is known the survival probability of the perfectly binding site in the channel, in the geometry of Fig. 1, can be expressed as

$$S_{l_1}(t)S_{l_2}(t)=\exp\left\{-c\int_0^t[k_{l_1}(\xi)+k_{l_2}(\xi)]d\xi\right\}. \quad (5.1)$$

This representation shows how the survival probability depends on the location of the site inside of the channel.

ACKNOWLEDGMENT

The authors are grateful to Dr. Attila Szabo for numerous very helpful discussions.

APPENDIX: FURTHER DETAILS OF THE SIMULATIONS

The geometric configuration used in our simulations is shown in Fig. 7. A circular cylinder of length L and radius equal to a is attached to a wall of a unit cube whose sides are perfectly reflecting as are the sides of the cylinder, except for its dead end, which is absorbing. Reflections from the walls were handled by returning the diffusing particle to the position it had just prior to hitting the wall. A comparison of results obtained by this simplified method, which saves a considerable amount of computer time, and those by a more accurate one were only slightly different.

In the simulations the cylinder length varied from 0 to 5, while the radius of the cylinder varied from 0.02 to 0.05. A given particle's motion both in the box and within the cylinder was determined by sampling from a Gaussian process. If

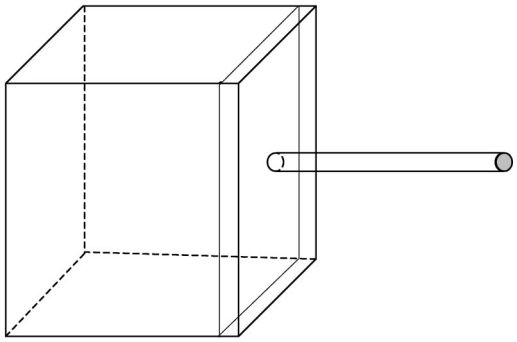

FIG. 7. Schematic diagram of the system configuration used in the simulations, consisting of a reflecting cube whose sides have a length equal to 1 with a cylinder attached at the center of one of the sides. The striped dead end of the cylinder is an absorbing surface while the circular side of the cylinder is reflecting. Also shown is the thin slab contacting the side containing the cylinder. Within this slab the time step is shorter than in the remainder of the cube.

$\boldsymbol{\xi}$ is a three-dimensional Gaussian random variable with zero mean and variance equal to 1/2, then the displacement in a single step is set equal to $(\Delta t)^{1/2}\boldsymbol{\xi}$. We used the values $\Delta t = 10^{-6}$ in the cylinder and in the thin slab of thickness 0.1 in contact with the wall containing the cylinder (cf. Fig. 7) and $\Delta t = 10^{-4}$ in the rest of the cube.

The rate coefficient was calculated as the inverse of the average time for a particle to be absorbed. Most of the results were obtained using 10^4 random walkers whose initial positions were uniformly distributed throughout the cube. Results for cylinders with $L = 2-5$ were obtained using 10^3 random walkers due to the very long running time for a single random walker.

[1] K. Brejc, W. J. van Dijk, R. V. Klaassen, M. Schuurmans, J. van der Oost, A. B. Smit, and T. K. Sixma, Nature (London) **411**, 269 (2001).
[2] C. Rosenmund and M. Mansour, Nature (London) **417**, 238 (2002).
[3] Y. Sun, R. Olson, M. Hornig, N. Armstrong, M. Mayer, and E. Gouaux, Nature (London) **417**, 245 (2002).
[4] D. B. Tikhonov, J. R. Mellor, P. N. R. Usherwood, and L. G. Magazanik, Biophys. J. **82**, 1884 (2002).
[5] D. E. Pellegrini-Giampietro, J. A. Gorter, M. V. L. Bennett, and R. S. Zukin, Trends Neurosci. **20**, 464 (1997).
[6] C. G. Parsons, W. Danysz, and G. Quack, Neuropharmacology **38**, 735 (1999).
[7] L. L. Zaulyanov, P. S. Green, and J. W. Simpkins, Cell Mol. Neurobiol. **19**, 705 (1999).
[8] E. M. Nestorovich, C. Danelon, M. Winterhalter, and S. M. Bezrukov, Proc. Natl. Acad. Sci. U.S.A. **99**, 9789 (2002).
[9] S. M. Bezrukov, A. M. Berezhkovskii, M. A. Pustovoit, and A. Szabo, J. Chem. Phys. **113**, 8206 (2000).
[10] A. M. Berezhkovskii, M. A. Pustovoit, and S. M. Bezrukov, J. Chem. Phys. **116**, 6216 (2002).
[11] A. M. Berezhkovskii, M. A. Pustovoit, and S. M. Bezrukov, J. Chem. Phys. **116**, 9952 (2002).
[12] T. H. Hill, Proc. Natl. Acad. Sci. U.S.A. **72**, 4918 (1975).
[13] H. C. Berg and E. M. Purcell, Biophys. J. **20**, 193 (1977).
[14] D. Shoup and A. Szabo, Biophys. J. **40**, 33 (1982).
[15] R. Zwanzig, Proc. Natl. Acad. Sci. U.S.A. **87**, 5856 (1990).
[16] R. Zwanzig and A. Szabo, Biophys. J. **60**, 671 (1991).
[17] R. Samson and J. M. Deutch, J. Chem. Phys. **68**, 285 (1978).
[18] D. Shoup, G. Lipari, and A. Szabo, Biophys. J. **36**, 697 (1981).
[19] E. R. Hansen, *A Table of Series and Products* (Prentice-Hall, Englewood Cliffs, NJ, 1975).